PNAS RESEARCH ARTICLE | BIOPHYSICS AND COMPUTATIONAL BIOLOGY

Polymer sailing on rafts within lipid membranes

Jie Gao[a,b], Yiyang Shen[c], Shigeyuki Komura[d], Wenbing Hu[b,1], Lei Shen[e,1], and Jinglei Hu[a,b,1]

Affiliations are included on p. 8.

Edited by Monica Olvera de la Cruz, Northwestern University, Evanston, IL; received February 17, 2025; accepted June 5, 2025

Understanding the dynamics of macromolecules adsorbed from extracellular fluids onto cell membranes is crucial for elucidating basic cellular processes and advancing applications in biotechnology, such as biosensing, therapeutics, and synthetic biology. However, this is complicated by the interplay between membrane heterogeneity, macromolecule conformation, and fluid hydrodynamics. We investigate the dynamics of linear polymers on binary lipid membranes using hydrodynamics simulations and single-molecule tracking experiments. We find that the preferential adsorption of nanosized polymer onto the raft-forming component of the membrane induces and stabilizes a single lipid raft that colocalizes with the polymer. This lipid raft, in turn, imposes dynamic confinement on the polymer, resulting in swollen yet restricted 2D conformations and Saffman–Delbrück-type diffusivity. These effects lead to an unusual scaling for polymer interfacial diffusion, $D \sim N^{-\nu_D}$ with $\nu_D \approx 0.5$. Normal mode analysis further reveals that the relaxation time of the polymer's slowest mode surprisingly follows the prediction of Zimm model for a 3D chain in a good solvent, irrespective of whether the polymer's hydrodynamics are dominated by the 3D solvent or 2D fluid membrane. We also identify two diffusive modes: Saffman–Delbrück-type for polymer on heterogeneous membranes and Stokes–Einstein-like for polymer on homogeneous membranes, demonstrating the potential of polymer adsorbates as biosensors for membrane heterogeneity. Our study provides insights into polymer dynamics on biological membranes and suggests that polymer adsorbates can modulate lipid rafts, influencing raft-related cellular processes.

adsorption | bilayer | diffusivity | lipid raft | dynamic confinement

Cell membranes are a ubiquitous kind of fluid surface, where biopolymers adsorbed from extracellular fluid exchange momentum with both the mobile lipids beneath them and the surrounding solvent, and diffuse laterally to perform biological functions. For instance, amyloid-β peptides adsorb to lipid-raft-associated gangliosides GM1 on neuronal membranes, where they form neurotoxic aggregates implicated in the pathogenesis of Alzheimer's disease (1–5). Disordered peptides and proteins are often membrane- or raft-associated and play critical roles in cellular processes (6–8). A central question is how the hydrodynamics within the fluid membrane (2D) and the surrounding solvent (3D), along with the lateral heterogeneity of the membrane (9–14), regulate the dynamics of adsorbed polymers.

Maier and Rädler (15) pioneered the investigation of DNA adsorbed onto a homogeneous, supported lipid membrane. They found that the DNA adopts 2D swollen conformations as evidenced by the scaling relation $R_g \sim N^{3/4}$ for its radius of gyration, while its center-of-mass diffusivity scales as $D \sim N^{-1}$ with its degree of polymerization N. In their experiments, the screening of hydrodynamic interactions (HI) at the membrane surface causes each monomer of the DNA to behave as an independent drag unit. Subsequent studies have primarily focused on solid surfaces (16–24), presumably because fluid surfaces were initially considered less intriguing than solid ones. A striking observation from these studies is the scaling $D \sim N^{-3/2}$ for the slowed diffusion of 2D swollen polymers, which has been attributed to polymer reptation (with a terminal relaxation time $\tau \sim N^3$, and hence $D \sim R_g^2/\tau \sim N^{-3/2}$) caused by obstacles or sticking sites at smooth solid surfaces (18, 21), or to the static barriers to diffusion arising purely from surface roughness (22). Molecular dynamics simulations have demonstrated a transition from $D \sim N^{-1}$ to $D \sim N^{-3/4}$ upon the inclusion of HI at smooth solid surfaces (19, 20). Interestingly, HI here leads to the Stokes–Einstein-like diffusivity $D \sim R_g^{-1}$ for the 2D swollen polymer.

In another study using homogeneous membranes, Zhang and Granick (25) found that the adsorption of quaternized poly-4-vinylpyridine onto supported

Significance

Biopolymer adsorption and diffusion on cell membranes are vital for cellular processes such as signal transduction and disease development, including Alzheimer's. However, the impact of membrane heterogeneity and fluid hydrodynamics on polymer dynamics remains poorly understood. We find that nanosized polymers adsorbed onto binary lipid membranes induce the in-situ formation of single lipid rafts, which impose dynamic constraints on the polymers. This leads to an unusual scaling law for polymer interfacial diffusion. We also identify two diffusive modes for polymer adsorbates on lipid membranes: Saffman–Delbrück-type and Stokes–Einstein-like, revealing their potential as biosensors for membrane heterogeneity. These findings provide insights into polymer–membrane interactions, with significant implications for biophysics and biotechnology, particularly in understanding membrane organization and advancing membrane-targeted therapeutic approaches.

The authors declare no competing interest.

This article is a PNAS Direct Submission.

[1]To whom correspondence may be addressed. Email: wbhu@nju.edu.cn, leishen@whut.edu.cn, or hujinglei@nju.edu.cn.

This article contains supporting information online at https://www.pnas.org/lookup/suppl/doi:10.1073/pnas.2503203122/-/DCSupplemental.

Published July 3, 2025.

1,2-dilauroyl-sn-glycero-3-phosphocholine membranes induces a population of lipids with reduced diffusivity that scales as $D_L \sim N^{-1}$. At water-polydimethylsiloxane oil interfaces, $D \sim N^{-2/3}$ was observed for poly(ethylene glycol) (26), attributed to a 2D partially swollen, loop-train-tail conformation of the polymer. The scaling $D \sim N^{-3/4}$ on smooth solid surfaces in the presence of HI (19, 20) was also observed for polymers confined at liquid–liquid interfaces from simulations (27). All these findings at solid and homogeneous fluid surfaces naturally raise fundamental questions: How do polymers behave when adsorbed onto cell membranes, particularly onto lipid rafts within the membrane like amyloid-β peptides? Could novel D-N scaling relations emerge in these systems? Does the adsorbed polymer exhibit the Stokes–Einstein-like (3D) or Saffman–Delbrück-type (2D, analogous to transmembrane proteins) (28) diffusivity?

Here, we investigated the behavior of linear polymers adsorbed onto binary lipid membranes by combining GPU-accelerated hydrodynamics simulations and single-molecule tracking experiments. The two-component membranes with dynamic lipid clusters serve as a minimal model for mimicking cell membranes, which contain highly dynamic, sterol- and sphingolipid-enriched clusters known as lipid rafts, ranging in size from about 10 to 100 nm (9, 11, 12). We find that the preferential adsorption of the polymer to raft-forming component of the membranes can induce and stabilize a raft-like cluster that colocalizes with the polymer. This raft cluster, in turn, imposes dynamic confinement on the polymer, leading to two effects: swollen yet restricted 2D conformations and Saffman–Delbrück-type diffusivity. Together, these effects result in a scaling law of polymer interfacial diffusion, $D \sim N^{-\nu_D}$ with $\nu_D \approx 0.5$. Surprisingly, the relaxation time of the polymer's first normal mode follows the prediction of Zimm model, $\tau_1 \sim N^{3\nu}$, for a 3D polymer in a bulk solvent (29, 30), regardless of whether the hydrodynamics of the polymer are dominated by the solvent (3D) or fluid membrane (2D). However, higher-order normal modes of the polymer on heterogeneous membranes deviate from Zimm model due to the influence of lipid clusters. Both Stokes–Einstein-like and Saffman–Delbrück-type diffusivities are observed for the polymer, indicating its ability to physically sense the membrane heterogeneity. Our findings provide insights into the dynamics of polymers adsorbed onto biological membranes and highlight the complex interplay between membrane heterogeneity, polymer conformation, and fluid hydrodynamics.

Results

Unusual Scaling Law for Polymer Diffusion on Lipid Rafts. The heterogeneity of lipid membranes influences the interfacial diffusion of polymer chains adsorbed onto them. Fig. 1 *B* and *C* shows the results from coarse-grained molecular dynamics (CGMD) simulations of one linear polymer immersed in water

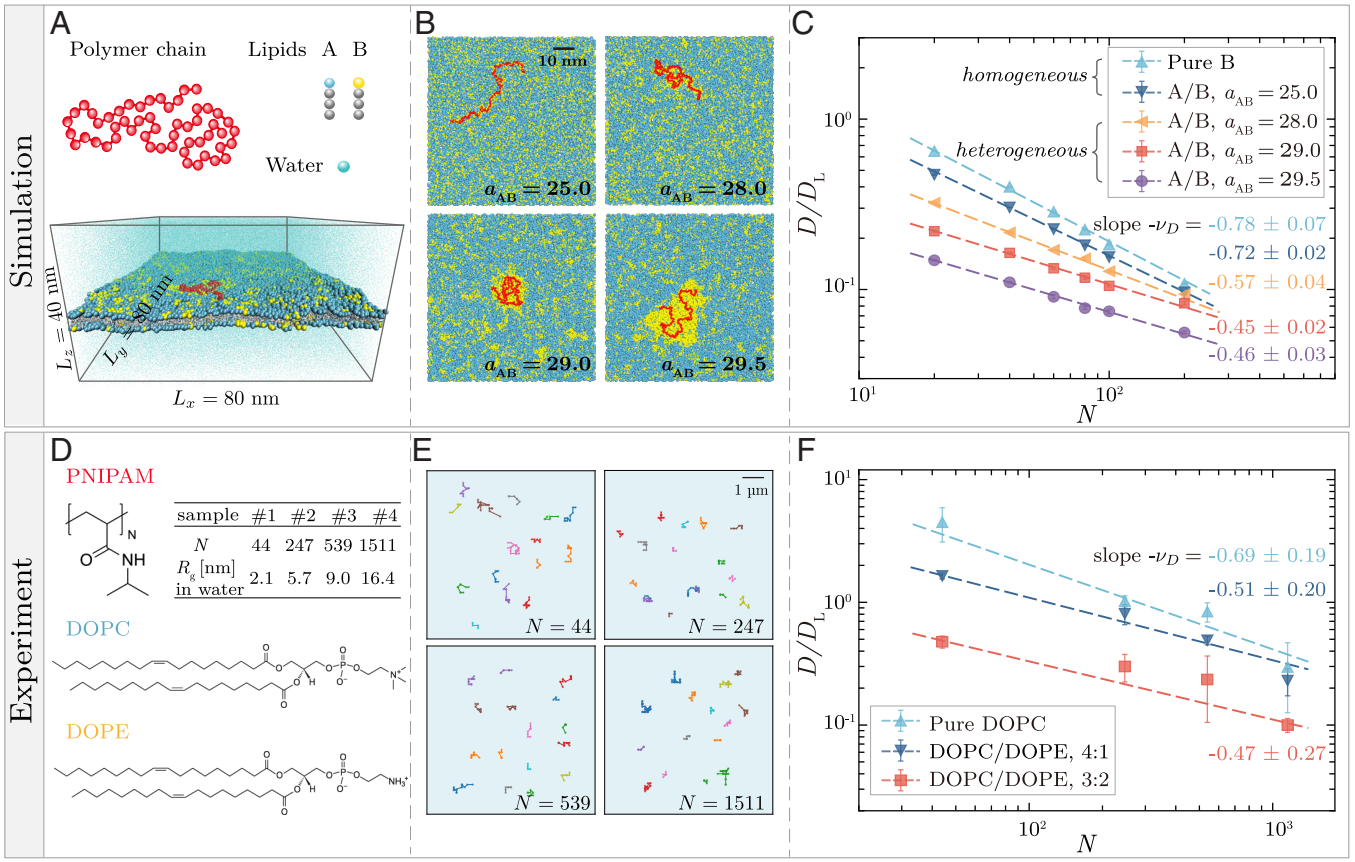

Fig. 1. Diffusion of single polymers on lipid membranes measured from simulations (*A*–*C*) and experiments (*D*–*F*). (*A*) Model of polymer, lipids, and water used in simulations. (*B*) Top view of simulation snapshots of a polymer (in red; with degree of polymerization $N = 200$) strongly adsorbed onto binary fluid membranes (A in sky blue and B in yellow) with fixed molar fraction $x_B = 0.2$ for the raft-forming component B but varying strengths of A–B repulsion a_{AB}. The polymer exhibits stronger affinity with B than with A. (*C*) Polymer diffusivity D rescaled by lipid diffusivity D_L against N. (*D*) Polymer and lipids used in experiments. (*E*) Typical trajectories of PNIPAM chains on DOPC/DOPE membranes with molar ratio of 3:2. (*F*) D/D_L versus N. DOPE forms clusters in the 4:1 and 3:2 membranes (*SI Appendix*, Fig. S3*A*). Dashed lines with specified slopes are least-squares fits to data points in (*C* and *F*). The errors of least-squares fitting are estimated using the jackknife method (see *SI Appendix* for the details).

and strongly adsorbed onto free-standing binary lipid membranes (Fig. 1*A*). The snapshots in Fig. 1*B* provide a Top view of the polymer (in red) on four membranes composed of lipids A (in sky blue) and B (in yellow), all with the same composition but varying strengths of A–B repulsion a_{AB}. The molar fraction of raft-forming component B is fixed at $x_B = 1 - x_A = 0.2$ (31). These membranes will be referred to as A/B hereafter. Each monomer of the polymer has a higher affinity with B than with A. As a_{AB} increases from 25.0 to 29.5 (in reduced units, with $a_{AA} = a_{BB} = 25.0$ fixed; see *SI Appendix* for details), the membrane, behaving like a 2D fluid, changes from a homogeneous, random-mixing state to a heterogeneous state with dynamic B clusters floating within the A matrix. If a_{AB} exceeds the threshold around 30.0, the A/B bilayer laterally separates into a single macroscopic B domain embedded within the majority A phase (see *SI Appendix*, Fig. S1 for details). The polymer preferentially adsorbs onto B and adjusts its conformation according to the membrane's state, which may result in deviations from the scaling laws for diffusion observed at solid (16–24) and fluid surfaces (15, 26, 27).

Fig. 1*C* displays the polymer's center-of-mass diffusivity D as a function of its degree of polymerization N in the four A/B membrane systems depicted in Fig. 1*B*. The polymer radius of gyration R_g ranges from about 1 to 10 nm. For comparison, data from the control system with the polymer on a pure B membrane are also included. The diffusion coefficient D_L of lipids in the pure B membrane is used to normalize D. Over the range of N explored in the simulations, the scaling relation $D \sim N^{-\nu_D}$ generally holds, as indicated by the fitted lines in the log–log plot. However, the exponent ν_D is clearly dependent on the system. The polymer on the pure B (in light blue) or homogeneous A/B membrane ($a_{AB} = 25.0$; in blue) has the scaling exponent $\nu_D = 0.78 \pm 0.07$ or 0.72 ± 0.02, consistent with the exponent $\nu_{R_g} = 0.80 \pm 0.01$ or 0.77 ± 0.01 in $R_g \sim N^{\nu_{R_g}}$ (Fig. 2*C*). These values are close to the Flory exponent $\nu_F = 3/4$ for a 2D self-avoiding chain. As a_{AB} further increases, the raft-forming component B starts to segregate from A and forms dynamic clusters within the membrane, slowing down the diffusion of the adsorbed polymer and leading to the following values of exponent ν_D: 0.57 ± 0.04 at $a_{AB} = 28.0$ (in orange), 0.45 ± 0.02 at $a_{AB} = 29.0$ (in red), and 0.46 ± 0.03 at $a_{AB} = 29.5$ (in purple). Unlike the case of pure B membrane or A/B membrane with $a_{AB} = 25.0$, the exponent ν_D is now smaller than the corresponding exponent ν_{R_g} (Fig. 2*C*). More surprisingly, the value of ν_D in the last two A/B membrane systems, where the polymer is confined within a single yellow raft (Fig. 1*B*), does not match any values reported in previous studies of polymers adsorbed onto solid or fluid surfaces. This discrepancy suggests that the dynamic confinement of the adsorbed polymer within the lipid raft leads to a distinct scaling law for polymer diffusion.

To validate our findings regarding polymer diffusion on rafts within lipid membranes, we conducted single-molecule tracking experiments to measure the diffusion of PNIPAM at the surface of DOPC/DOPE membranes (Fig. 1 *D*–*F*). The DOPC/DOPE membrane system is widely used and has been shown to undergo lateral phase separation with increasing molar fraction of DOPE up to 0.65 (32). In this study, we selected DOPC/DOPE membranes with molar ratios of 4:1 and 3:2, both smaller than the threshold for phase separation. To complement the tracking experiments, we performed 1 μs all-atom molecular dynamics (AAMD) simulations of the two membranes, confirming that DOPE forms dynamic clusters in both membranes, with larger average cluster size observed in the 3:2 membrane (see *SI Appendix*, Fig. S3*A* for details). It is worth mentioning that accurately assessing the diffusion of single PNIPAM chains on the membranes using AAMD simulations remains computationally infeasible.

Fig. 1*F* presents the diffusion coefficient D of the PNIPAM chain at the water–membrane interface as a function of N, measured from our tracking experiments. Each data point was derived from over 10^3 trajectories as shown in Fig. 1*E*. In the control system with a pure DOPC membrane (in light blue), the PNIPAM chain can diffuse even faster than the lipid, i.e., $D/D_L > 1$, implying rather weak adsorption of the polymer on DOPC. The exponent $\nu_D = 0.69 \pm 0.19$ in $D \sim N^{-\nu_D}$ is close to the value of approximately 2/3 observed for poly(ethylene glycol) at the water–oil interfaces (26). As more DOPE is added to the DOPC membranes (in blue and red), the diffusion of PNIPAM slows down significantly, reflecting a much stronger affinity of PNIPAM for DOPE than for DOPC. The scaling exponent $\nu_D = 0.47 \pm 0.27$ for the 3:2 membrane agrees with our CGMD simulation results (red and purple data in Fig. 1*C*). The single-molecule tracking experiments confirmed our findings that polymers on nanoscale rafts within lipid membranes exhibit unusual scaling of diffusion.

Conformation of the Polymer Confined within Lipid Rafts. The time sequence of simulation snapshots in Fig. 2*A* illustrates that the polymer (in red; with $N = 200$) adapts its conformation to the surrounding B raft (in yellow). All the B clusters (distinguished by different colors) floating within the matrix of A (in sky blue) constantly undergo fusion and fission, resulting in changes in their size and shape, as well as the annihilation of old clusters and the emergence of new ones. These transient clusters arise from thermal fluctuations, in contrast to the domain growth below the transition temperature, which leads to macroscopic phase separation either via nucleation and growth or via spinodal decomposition. The number of B lipids within the yellow raft that adheres to the polymer changes over time (*SI Appendix*, Fig. S4). Fig. 2*B* shows that the average number of B lipids in this raft increases with N and fits well to $\bar{N}_B = N_{B,0} + c_N N^{2\nu_{R_g}}$, where the offset $N_{B,0}$ accounts for the cluster size in the absence of polymer adsorption, and $c_N N^{2\nu_{R_g}}$ is proportional to the effective area occupied by the polymer. The fitted values of $N_{B,0}$ are greater than the average number of B lipids within all clusters in the naked membranes, which are 22 at $a_{AB} = 29.0$ and 48 at $a_{AB} = 29.5$, implying that the adsorbed single polymer acts as a macromolecular glue, binding small clusters together into a large raft. With the fitted values of $c_N = 0.57$ and 0.35, the $c_N N^{2\nu_{R_g}}$-term is found to exceed the number of lipids in a B cluster occupying the same area as that covered by the polymer, $\pi R_g^2 / A_L$, where $A_L \approx 0.8$ nm^{-2} is the area per lipid in the membranes. These numbers are $0.25\, N^{2\nu_{R_g}}$ at $a_{AB} = 29.0$ and $0.19\, N^{2\nu_{R_g}}$ at $a_{AB} = 29.5$. These results, together with the distributions of B cluster size without and with the adsorbed polymer in *SI Appendix*, Fig. S1*D*, clearly show that the adsorption of the polymer to heterogenous A/B membranes (with $a_{AB} = 29.0$ or 29.5) induces and stabilizes a mobile B raft that colocalizes with the polymer. This lipid raft, in turn, will impose dynamic confinement on the polymer.

Fig. 2 *C* and *D* shows the polymer radius of gyration R_g and end-to-end distance R_e as a function of N. The slopes of the fitted lines in these log–log plots correspond to the exponents ν_{R_g} and ν_{R_e} in $R_g \sim N^{\nu_{R_g}}$ and $R_e \sim N^{\nu_{R_e}}$. Confinement of the polymer by the lipid raft in A/B membranes with $a_{AB} = 29.0$ or 29.5 leads

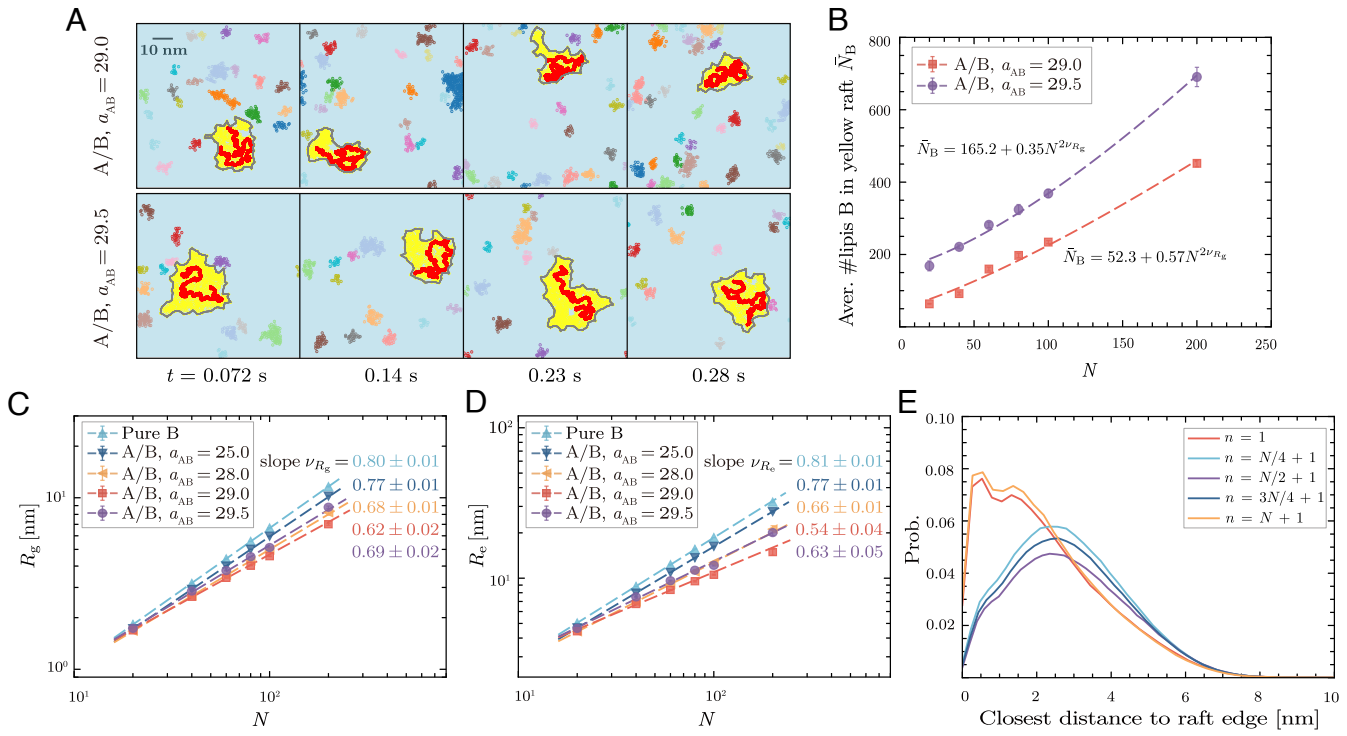

Fig. 2. Conformation of single polymers on different membranes from simulations. (*A*) Time sequence of snapshots for a polymer with $N = 200$ on heterogeneous A/B membranes with $a_{AB} = 29.0$ and 29.5. The polymer in red is confined within the B raft in yellow, while other B clusters are illustrated in distinct colors. The matrix of A is colored in sky blue as the background. (*B*) Average number of B lipids within the yellow raft against *N*. (*C* and *D*) Polymer radius of gyration R_g and end-to-end distance R_e against *N*. (*E*) Distribution of the closest distances of individual monomers to the edge of the yellow raft in the A/B membrane with $a_{AB} = 29.0$.

to reductions in R_g and R_e, as well as decreases in ν_{R_g} and ν_{R_e}, compared to the pure B or A/B (with $a_{AB} = 25.0$) membrane system, in which lipids are in a random-mixing state. For the A/B membrane with $a_{AB} = 28.0$, the adsorbed polymer links multiple small lipid clusters (Fig. 1*B*). The size of the polymer and the two scaling exponents in this case are similar to those observed on the A/B membrane with $a_{AB} = 29.5$, as the polymer confined within the large raft at $a_{AB} = 29.5$ has more conformational freedom compared to that in the raft at $a_{AB} = 29.0$. These results demonstrate that the association of the polymer with B clusters effectively weakens the solvent-mediated monomer–monomer repulsion, leading to swollen yet restricted 2D conformations of the polymer.

A close inspection of Fig. 2 *C* and *D* reveals that, for the polymer on the A/B membrane with $a_{AB} = 29.0$, the scaling exponents satisfy the inequality $\nu_{R_g} > \nu_{R_e}$, i.e., R_e of the polymer confined within a lipid raft is less sensitive to N than R_g. To corroborate that this observation is a generic feature of a polymer strongly confined within a lipid cluster, we performed large-scale Monte Carlo (MC) simulations of a 2D lattice model, which serves as a simplified representation of our coarse-grained molecular model used in MD simulations (see *SI Appendix*, Fig. S3*B* for details). This 2D lattice enables the investigation of much longer polymer chains, with N up to 2,000 and R_g up to about 30 nm, adsorbed onto micron-sized heterogeneous membrane surfaces. Similar results from these MC simulations, as shown in *SI Appendix*, Fig. S5, confirm that R_e of the polymer confined within a lipid cluster is indeed less sensitive to N than R_g, a behavior that may extend to polymers confined in spheres or other 3D geometries (33–36). To further understand this phenomenon, we analyzed the distribution of the closest distances of individual monomers to the edge of the dynamic lipid raft from CGMD simulations of the A/B membrane system with $a_{AB} = 29.0$, as shown in Fig. 2*E*. The terminal monomers ($n = 1$ and $N + 1$) that determine R_e preferentially localize near the cluster edge compared to the internal monomers, reducing the sensitivity of R_e to N. To access as many conformations as possible under the dynamic confinement by the raft, the two end monomers, which are more mobile than the internal monomers, remain close to the raft edge. This allows them to follow the dynamic shape of the raft.

Polymer Relaxation Dynamics. To investigate the relaxation dynamics of the polymer on different A/B membranes, we conducted normal mode analysis by deriving the normal coordinates $\mathbf{q}_i(t) = \frac{1}{N+1}\sum_n \cos\frac{in\pi}{N+1}\mathbf{r}_n(t)$ from Cartesian coordinates $\mathbf{r}_n(t)$ of the monomers, indexed by $n = 1, 2, ..., N + 1$. The autocorrelation function of $\mathbf{q}_i(t)$ is approximated by an exponential decay, $\langle \mathbf{q}_i(0) \cdot \mathbf{q}_i(t)\rangle = \langle \mathbf{q}_i^2\rangle e^{-t/\tau_i}$, where τ_i is the relaxation time of the i-th mode. Fig. 3*A* displays τ_1 as a function of N. The slope of the fitted line for each membrane system yields the exponent ν_{τ_1} in $\tau_1 \sim N^{\nu_{\tau_1}}$. The *Inset* shows that ν_{τ_1} agrees with $3\nu_{R_g}$ within 10%. The Zimm model for a 3D polymer in a good solvent predicts $\tau_i \sim (N/i)^{3\nu_{R_g}}$ (29, 30), which reduces to $\tau_1 \sim N^{3\nu_{R_g}}$ for the slowest mode $i = 1$. $\log_2(\tau_1/\tau_2)$ and $\log_3(\tau_1/\tau_3)$ are plotted against $3\nu_{R_g}$ in Fig. 3 *B* and *C*. Over the range of N examined in our simulations, data points of pure B membrane system (in light blue) and A/B membrane system with $a_{AB} = 25.0$ (in blue) align with the Zimm model, whereas those of A/B systems with $a_{AB} = 28.0$ (in orange), 29.0 (in red), and 29.5 (in purple) exhibit significant deviations.

The normal mode analysis revealed that the slowest relaxation mode ($i = 1$) is consistent with the Zimm model across various membrane systems, while higher modes ($i = 2$ and 3), which are more sensitive to the polymer's local conformational details, deviate from the Zimm model when the A/B membranes are heterogeneous ($a_{AB} = 28.0$, 29.0, and 29.5). These findings remain consistent when ν_{R_g} is replaced by ν_{R_e}, as shown in *SI Appendix*, Fig. S6 *A–C*.

To relate the relaxation dynamics of the adsorbed polymer to its center-of-mass diffusion, we plotted the ratio of the square of the radius of gyration, R_g^2, to the center-of-mass diffusion coefficient, D, as a function of the relaxation time τ_1, as shown in Fig. 3*D*. Data from various membrane systems all fit well to the empirical equation $R_g^2/D = c_\tau \tau_1$, where the coefficients c_τ, associated with the intercepts of the fitted lines, vary across different systems. Comparing our results with the equation $R_g^2/D = 4\tau_1$ reported for adsorbed polymers at solid surfaces (22) suggests that the scaling relation $D \sim R_g^2/\tau_1$ is generally applicable to adsorbed polymers, although the proportionality coefficient depends on the characteristics of the surface. Similar conclusions hold when τ_1 is replaced by the relaxation time τ_e of the end-to-end vector, as shown in *SI Appendix*, Fig. S6*D*.

As illustrated in Fig. 2*A*, the yellow lipid raft in the A/B membrane with $a_{AB} = 29.0$ exhibits a highly dynamic morphology that confines the polymer. A natural question arises as to whether fluctuations in the shape of the cluster affect the polymer dynamics. To this end, we performed additional simulations using the A/B membrane with $a_{AB} = 100.0$, which laterally separates into a single B domain embedded in the majority A phase. The strong A–B repulsion largely suppresses the shape fluctuations of the B domain, resulting in a nearly circular morphology. By adjusting the molar fraction of lipids B, we ensured that, for each value of N, the size of the B domain was equal to the average radius of gyration of the B raft surrounding the polymer on the A/B membrane with $a_{AB} = 29.0$. The results in Fig. 3*A* reveal that the polymer confined in the B domain (empty squares) has a shorter relaxation time τ_1 than that in the dynamic raft (filled squares), while the scaling exponents ν_{τ_1} remain the same. These additional simulations indicate that shape fluctuations of the lipid raft facilitate the confined polymer's access to more conformations and therefore decelerate its relaxation dynamics.

Size Dependence of Polymer Diffusivity: Stokes–Einstein-Like and Saffman–Delbrück-Type. The diffusion coefficient D of the polymer is plotted against its radius of gyration R_g in Fig. 4*A*. The data from pure B membrane system (in light blue) and homogeneous A/B membrane system ($a_{AB} = 25.0$; in blue) conform to the Stokes–Einstein-like (SE-like) relation $D = k_B T/(c\pi\eta_s R_g)$ with the single fitted parameters $c = 6.20$ and 8.80, suggesting that the adsorbed polymer behaves hydrodynamically as a 3D object. This finding contrasts with the intuition that small objects attached to or embedded in membranes should exhibit the Saffman–Delbrück-type diffusivity like transmembrane proteins (28, 37, 38), as discussed further below. In our CGMD simulations, the solvent viscosity $\eta_s = 0.866$ (in reduced units; *SI Appendix* text) (39) is constant across all membrane systems. Both the pure B and homogeneous A/B membranes have the same viscosity ($\eta_m/\eta_s = 2.65$; *SI Appendix* text), as the B–B, A–B, and A–A interactions are identical (*SI Appendix*, Table S1). During diffusion, each monomer of the polymer either moves with the lipid to which it is adsorbed or hops to an adjacent lipid. On the homogeneous A/B membrane, the hopping of monomers from more attractive B sites to less attractive A sites is accompanied by energy penalties that are absent on the pure B membrane, resulting in stronger effective friction between the polymer and the A/B membrane. As a result, a larger value of c is observed on A/B membrane with $a_{AB} = 25.0$.

As previously noted, the scaling exponent ν_D in $D \sim N^{-\nu_D}$ differs from ν_{R_g} in $R_g \sim N^{\nu_{R_g}}$ for the heterogeneous A/B membrane systems ($a_{AB} = 28.0$, 29.0, and 29.5). Data from these three systems (orange, red, and purple points in Fig. 4*A*) fit well to the Saffman–Delbrück (SD) equation (28, 40)

$$D = \frac{k_B T}{4\pi\eta_m \ell_m}\left(\ln\frac{\eta_m \ell_m}{\eta_s R_g} + 1/2 - \gamma\right), \qquad [1]$$

where $\ell_m = 4.5$ nm is the membrane thickness, and $\gamma \approx 0.57721$ is Euler's constant. The fitted membrane viscosities $\eta_m = 2.56$, 5.24, and 9.68 increase with the A–B repulsion strength a_{AB}. As illustrated in Fig. 1*B*, the polymer diffuses along with multiple B clusters at $a_{AB} = 28.0$, or with single B raft at $a_{AB} = 29.0$ and 29.5, meaning that the lipids within these B clusters move collectively with the polymer. As a_{AB} increases, the B clusters grow larger, and the polymer experiences stronger friction due to the increased A–B repulsion. Consequently, the effective membrane viscosity η_m sensed by the polymer increases with a_{AB}. All three fitted values of η_m exceed the solvent viscosity η_s, consistent with the fact that lipid membranes are more viscous than the solvent. The Saffman–Delbrück length, beyond which the polymer's friction with the solvent dominates the dissipation, is given by $\ell_{SD} = \eta_m \ell_m/(2\eta_s)$, with values of 6.7, 13.6, and 25.2 nm for the three heterogeneous A/B membrane systems, respectively. These values are consistent with realistic estimates on the order of 10 to 100 nm, given the typical surface viscosity $\eta_m \ell_m \sim 10^{-10}$ Pa·m·s for fluid membranes (41, 42) and the viscosity $\eta_s \sim 10^{-3}$ Pa·s for biological fluids (43).

The SD equation was originally formulated for the diffusion of a rigid cylinder embedded in a viscous bilayer membrane surrounded by solvent (28), and extended to describe the diffusivity of transmembrane proteins (44, 45) and microsized lipid domains in bilayers (40). Remarkably, the SD equation is also applicable to flexible polymers on heterogeneous membranes. In this context, D decreases logarithmically with R_g, slower than the $1/R_g$ dependence in the SE-like relation. This behavior explains why the exponent ν_D in $D \sim N^{-\nu_D}$ is smaller than ν_{R_g} in $R_g \sim N^{\nu_{R_g}}$ in the heterogeneous A/B membrane systems with $a_{AB} = 28.0$, 29.0, and 29.5 (orange, red, and purple data in Figs. 1*C* and 2*C*).

Fig. 4 *B–D* summarizes three scenarios for polymer diffusion on lipid membranes. The size dependence of polymer diffusivity is governed by viscous drag from both polymer–solvent (P–S) and polymer–membrane (P–M) interactions: When P–S friction predominates, the polymer diffuses as a 3D object in bulk solvent, following a SE-like relation; when P–M friction prevails, the polymer behaves analogously to a membrane inclusion, with its diffusivity described by the SD model. For a polymer diffusing on the pure A (or B) or homogeneous A/B membrane (Fig. 4*B*), each monomer of the polymer either moves with the lipid to which it is adsorbed or hops to a neighboring lipid. In this case, the lipids do not move collectively with the polymer, suggesting that P–M friction might be weaker than P–S friction, despite the membrane being more viscous than the solvent. To test this hypothesis, we attempted to fit the data from pure B membrane and homogeneous A/B membrane systems at $R_g < \ell_{SD} = 5.9$ nm (the leftmost three light-blue points and three blue points in

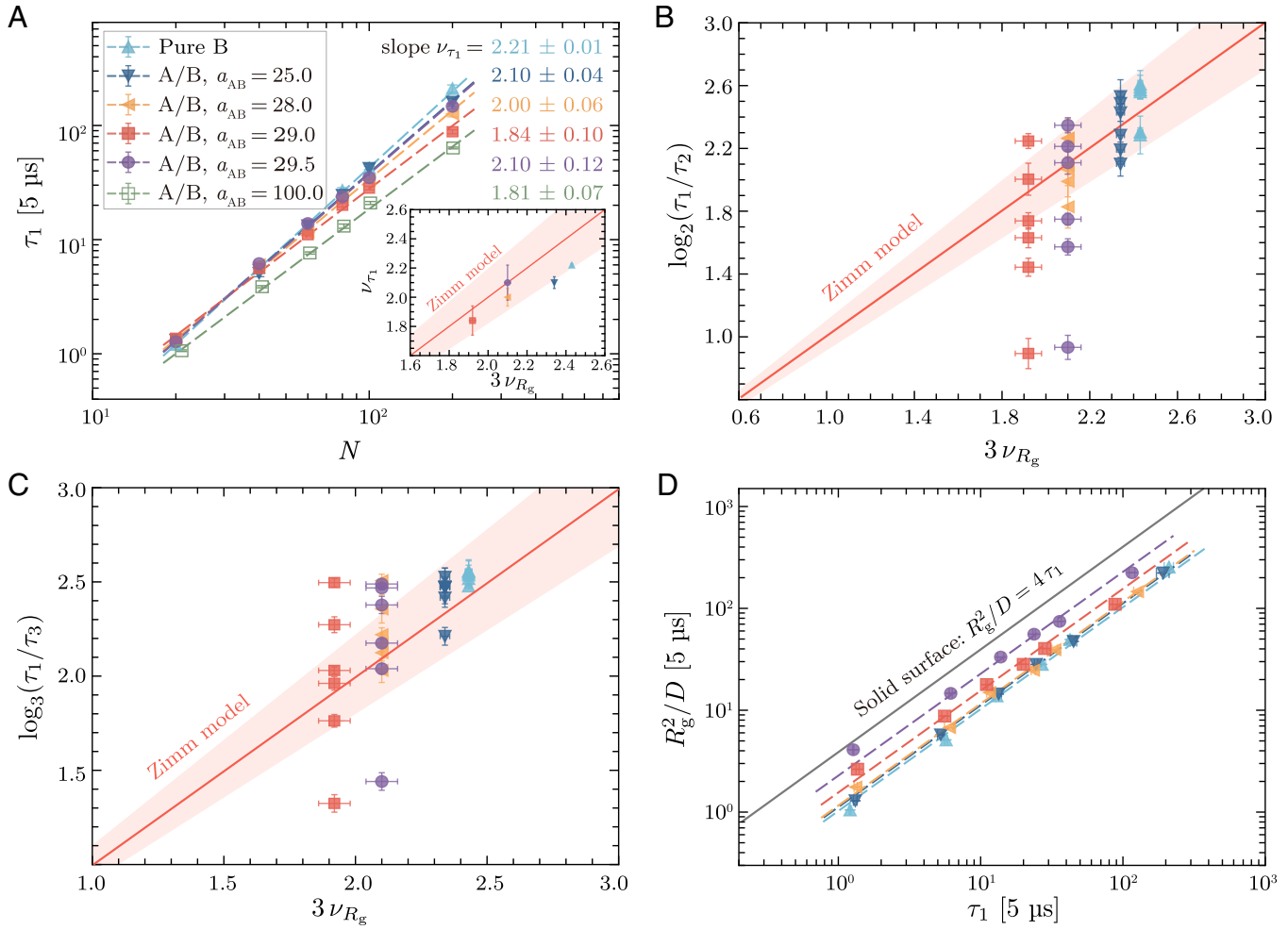

Fig. 3. Relaxation dynamics of polymers on different membranes from normal mode analysis. (*A*) τ_1 versus *N*. *Inset*: ν_{τ_1} versus $3\nu_{R_g}$, where ν_{τ_1} and ν_{R_g} are the exponents in $\tau_1 \sim N^{\nu_{\tau_1}}$ and $R_g \sim N^{\nu_{R_g}}$. (*B*) $\log_2(\tau_1/\tau_2)$ versus $3\nu_{R_g}$. (*C*) $\log_3(\tau_1/\tau_3)$ versus $3\nu_{R_g}$. τ_i is the relaxation time of the polymer's *i*-th mode. Shaded areas in (*A–C*) enclose the predictions within 10% deviation from the Zimm model. (*D*) R_g^2/D versus τ_1. Dashed lines are least-squares fits of data points to $R_g^2/D = c_\tau \tau_1$.

Fig. 4*A*) to the SD Eq. **1**, using the membrane viscosity η_m as the only fitting parameter. The least-squares fits (dashed light-blue and blue lines) deviate significantly from the data, supporting the hypothesis that P–S friction dominates in these two systems. If P–M friction were the primary source of dissipation, the SD Eq. **1** would better capture the polymer diffusivity. For a polymer to diffuse along with multiple B clusters or single B raft (in yellow) on a heterogeneous membrane (Fig. 4 *C* and *D*), the lipids within these B clusters move collectively with the polymer and experience strong friction from surrounding lipids. In this case, P–M friction prevails for short polymers ($R_g < \ell_{SD}$; Fig. 4*C*). However, when $R_g > \ell_{SD}$, the 3D flow of the solvent takes over the hydrodynamics (37, 38, 46, 47), resulting in SE-like diffusivity (Fig. 4*D*). The scenarios in Fig. 4 *B* and *C* correspond to the systems investigated in this study. Verification of the scenario shown in Fig. 4*D* requires future simulations of much longer polymers ($R_g > \ell_{SD}$) adsorbed onto larger lipid membranes.

Discussion

We have investigated the dynamics of single linear polymers adsorbed onto binary lipid membranes by combining GPU-accelerated hydrodynamics simulations and single-molecule tracking experiments. We find an unusual scaling law for polymer diffusivity, $D \sim N^{-\nu_D}$ with $\nu_D \approx 0.5$, when the polymer is confined by a lipid raft within the membrane (Fig. 1). To the best of our knowledge, this scaling behavior has not been previously observed in studies of polymer diffusion on solid or fluid surfaces, and originates from the dynamic confinement imposed by the raft. Nanosized biopolymers adsorbed from the cytosol or extracellular fluid onto lipid rafts are expected to obey the above scaling relation.

The scaling $D \sim N^{-\nu_D}$ with $\nu_D \approx 0.5$ holds for the regime that is set by two length scales: the Saffman–Delbrück length ℓ_{SD} on the order of 10 to 100 nm and the minimum size ℓ_c required for the polymer to induce a raft. ℓ_c can be roughly estimated via the geometric relation $\pi\ell_c^2 \sim 10A_L$, assuming that the minimal raft, induced by and associated with the adsorbed polymer, includes at least 10 lipids. For the typical area per lipid $A_L \approx 1$ nm^2, $\ell_c \sim 1.8$ nm. For a polymer chain with $R_g < \ell_c$, i.e., in the small-size regime, the chain is too short to induce a raft and behaves as a 2D self-avoiding walk with $R_g \sim N^{3/4}$ and diffusivity following the SE-like scaling $D \sim R_g^{-1} \sim N^{-3/4}$. In the large-size regime ($R_g > \ell_{SD}$), although the polymer chain induces rafts and exhibits swollen yet restricted 2D conformations with $R_g \sim N^{\nu_{R_g}<3/4}$, it follows the SE-like diffusivity $D \sim R_g^{-1} \sim N^{-\nu_{R_g}}$ as the 3D flow of the solvent takes

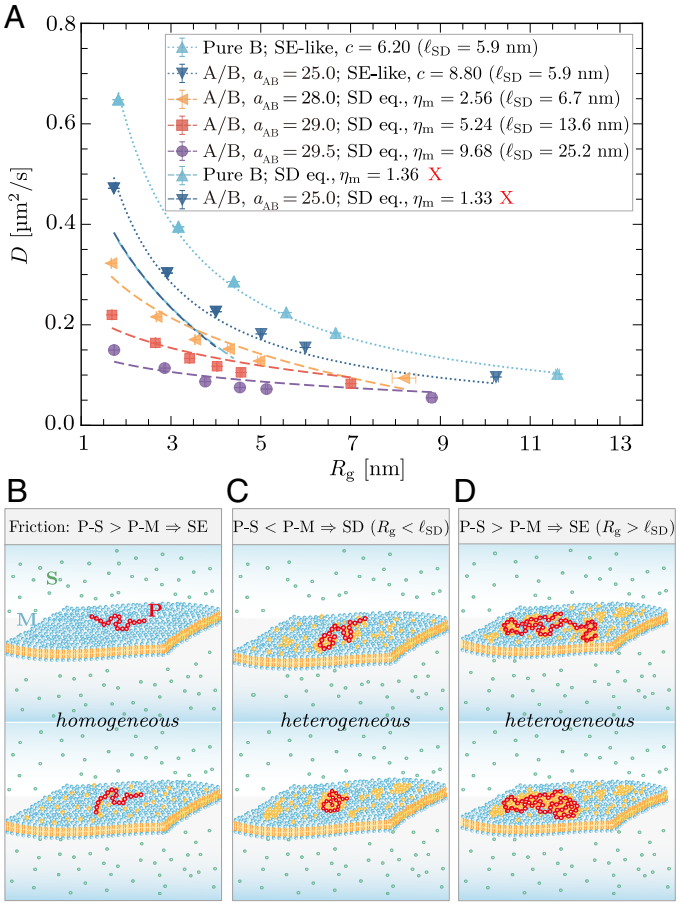

Fig. 4. Size dependence of polymer diffusivity. (*A*) D versus R_g. Dotted and dashed lines are least-squares fits of data points to Stokes–Einstein-like relation and Saffman–Delbrück Eq. **1**, respectively. The single fitted parameters c and η_m used for each dataset are discussed in the main text. (*B–D*) Illustration of three scenarios for polymer diffusion on membranes: The first two correspond to the systems investigated in this study, while the last one is expected for long polymers.

over the hydrodynamics. The scaling $D \sim N^{-\nu_D}$ with $\nu_D \approx 0.5$ therefore characterizes a nanosize, biologically relevant regime, and should not be interpreted as a crossover effect.

Another surprising finding is that the polymer's relaxation time τ_1 of the slowest normal mode scales as $\tau_1 \sim N^{3\nu}$ (with $\nu = \nu_{R_g}$ or ν_{R_e}), consistent with the Zimm model, regardless of whether the polymer is adsorbed onto homogeneous or heterogeneous membranes (Fig. 3). The size dependence of polymer diffusivity reveals that the polymer's hydrodynamics on homogeneous or heterogeneous membranes are dominated by the solvent (3D) or fluid membrane (2D), respectively (Fig. 4). In this context, it is particularly striking that the scaling $\tau_1 \sim N^{3\nu}$, originally predicted for a 3D polymer in a bulk solvent, still holds in both types of membrane systems.

These findings not only demonstrate that lipid membranes provide an intriguing fluid surface for exploring the dynamics of 2D polymers, a fundamental task in polymer physics but also stimulate further development of hydrodynamic theory for polymers on lipid membranes.

We now discuss our findings from the standpoint of membrane biophysics. On the one hand, the adsorbed polymer functions as a macromolecular glue, binding small lipid clusters together into a larger raft when the adsorption energy compensates for the loss in both lipid mixing entropy and polymer conformational entropy (Fig. 2). Recent studies by Veatch and Machta groups (48, 49) report clustering and signaling of cell membrane receptors induced by lipid rafts. Our previous study demonstrates that lipid rafts facilitate the formation of clusters of TCR–MHCp complexes in immunological synapse (50). The present study suggests that nanosized polymer adsorbates may offer a promising means to modulate such raft-associated processes (51). Lipid rafts, which are dynamic nanoscale clusters, form due to concentration fluctuations in multicomponent membrane systems that are above, but near, the phase separation point (52). In the systems studied here, the adsorption of single polymers hardly shifts the phase separation point, but can induce and stabilize a lipid raft that colocalizes with the polymer.

On the other hand, the diffusivity of membrane inclusions is a central concept in membrane biophysics, providing valuable insights into the structural and functional properties of biological membranes. Our findings of both Stokes–Einstein-like (SE-like) and Saffman–Delbrück-type (SD-type) diffusivities offer perspectives on how the 2D membrane and 3D solvent hydrodynamics regulate the diffusion of nanosized objects attached to membranes (Fig. 4). The observation of SE-like diffusivity for polymers on homogeneous membranes contrasts with the theoretical prediction of SD-type diffusivity for polymers embedded in lipid membranes by Ramachandran et al., who modeled the membrane as a continuum medium while neglecting its bilayer structure. Naji et al. postulated that local bumps of the membranes caused by inclusions could generate additional flows in the solvent, leading to SE-like

diffusivity (53, 54). In our systems, both polymer adsorption and thermal undulations may generate bumps of the free-standing membranes. However, if this mechanism were applicable, SE-like diffusivity would also be expected for polymers on heterogeneous membranes, which we do not observe. Our explanation is that adsorbed polymers can diffuse on homogeneous membranes via surface hopping of individual monomers rather than through collective motions of the lipids beneath them, unlike transmembrane proteins. In contrast, for polymers on heterogeneous membranes, their lateral diffusion is coupled to the collective motions of lipids in the associated clusters, resulting in SD-type diffusivity.

Our study demonstrates that polymers on multicomponent lipid membranes exhibit diffusive behavior distinct from that on conventional surfaces. Lateral membrane heterogeneity plays a crucial role in this behavior. In addition to their intrinsic heterogeneity, biological membranes are often subjected to active forces resulting from cytoskeletal deformations or conformational changes in transmembrane proteins (55). Investigating the dynamics of polymers on such active membranes and exploring the underlying nonequilibrium biophysics will also be an exciting direction.

Materials and Methods

Coarse-Grained Molecular Dynamics Simulations. We performed simulations using dissipative particle dynamics (56–58), a CGMD technique that reproduces the correct hydrodynamics (58, 59) and has been widely used to investigate the dynamics of polymer chains (21, 58, 60, 61) as well as lipid membranes (62–65). Our simulations of single polymer chains adsorbed onto two-component lipid membranes include water beads, lipid molecules, and a linear polymer chain (Fig. 1*A*). Each of the two types of lipid molecules, A and B, consists of one hydrophilic head bead and three hydrophobic tail beads, with any two adjacent beads bonded via harmonic springs. The polymer comprises a linear chain of beads connected by nonlinear springs. All pairs of beads of the polymer, lipids, and water softly repel each other with a strength that depends on the bead types. The polymer beads have stronger affinity with head beads of B than with head beads of A. The state of the two-component membranes, either homogeneous or heterogeneous, is governed by the effective repulsion strength between A and B lipids. We employed the highly optimized packages HOOMD-blue (66, 67) and PYGAMD (68, 69) to run GPU-accelerated CGMD simulations, and obtained polymer conformation and dynamics with high accuracy at a computationally affordable cost. Further details of the CG model, force field, validation, and setups of different membrane systems are provided in *SI Appendix*.

Single-Molecule Tracking Experiments. We measured the diffusion coefficient of fluorescently labeled PNIPAM chains at the interface between water and DOPC or DOPC/DOPE bilayers by tracking the trajectories of individual chains using total internal reflection fluorescence microscopy (TIRFM) (70). First, fluorescent dyes were covalently attached to the specific ends of the PNIPAM chains with a 1:1 stoichiometry. Four PNIPAM samples were used, all with a polydispersity index of approximately 1.5. The number-averaged molar masses (M_n) of the four samples were 5, 28, 61, and 171 kDa. The degree of polymerization N and root-mean-squared radius of gyration R_g in water are provided in Fig. 1*D*, following the scaling $R_g \sim N^{0.58}$ with the exponent close to the Flory exponent $\nu_F = 3/5$ for a 3D chain swollen in a good solvent. Second, fluid DOPC bilayers were prepared by depositing a solution of small unilamellar vesicles onto hydrophilically modified glass coverslips. DOPC/DOPE bilayers were formed by incorporating various amounts of DOPC lipids into the DOPC bilayers. Finally, fluorescently labeled PNIPAM chains were introduced to the DOPC or DOPC/DOPE bilayers and subjected to TIRFM measurements. More than 1,000 trajectories of individual PNIPAM chains were recorded for each experimental system. From each trajectory, the diffusion coefficient of the corresponding chain was extracted. The average diffusion coefficient over all tracked chains in each system is presented in Fig. 1*F*. Experimental details can be found in *SI Appendix*.

Data, Materials, and Software Availability. All study data are included in the article and/or *SI Appendix*. The Python scripts and initial configuration files for HOOMD-blue and PYGAMD simulations can be found in GitHub (71).

ACKNOWLEDGMENTS. Financial support from the National Natural Science Foundation of China (Grant Nos. 22473058, 22433002, 12232019, 22161132012, and 22173070), the Strategic Priority Research Program of Chinese Academy of Sciences (Grant Nos. XDB0620101, XDB0910301), and the National Key Research and Development Program of China (Grant No. 2023YFB3813001) is gratefully acknowledged. Part of our hydrodynamics simulations were performed at the computing facilities of the High Performance Computing Center of Nanjing University.

Author affiliations: [a]Kuang Yaming Honors School, Nanjing University, Nanjing 210023, China; [b]Department of Polymer Science and Engineering, Key Laboratory of High Performance Polymer Material and Technology of Ministry of Education, School of Chemistry and Chemical Engineering, Nanjing University, Nanjing 210023, China; [c]Department of Chemistry, School of Chemistry and Chemical Engineering, Nanjing University, Nanjing 210023, China; [d]Wenzhou Institute, University of Chinese Academy of Sciences, Wenzhou 325001, China; and [e]Department of Chemistry, School of Chemistry, Chemical Engineering and Life Sciences, Wuhan University of Technology, Wuhan 430070, China

Author contributions: J.H. conceived and designed research; J.G. and Y.S. performed simulations; L.S. conducted experiments; J.G., Y.S., S.K., W.H., L.S., and J.H. analyzed data; J.G., S.K., W.H., L.S., and J.H. wrote the paper; and J.H. supervised the project.

1. K. Yanagisawa, A. Odaka, N. Suzuki, Y. Ihara, GM1 ganglioside-bound amyloid ß-protein (aß): A possible form of preamyloid in Alzheimer's disease. *Nat. Med.* **1**, 1062–1066 (1995).
2. K. Yanagisawa, Role of gangliosides in Alzheimer's disease. *Biochim. Biophys. Acta Biomembr.* **1768**, 1943–1951 (2007).
3. C. Poojari, A. Kukol, B. Strodel, How the amyloid-ß peptide and membranes affect each other: An extensive simulation study. *Biochim. Biophys. Acta Biomembr.* **1828**, 327–339 (2013).
4. T. Matsubara *et al.*, Size and shape of amyloid fibrils induced by ganglioside nanoclusters: Role of Sialyl oligosaccharide in fibril formation. *Langmuir* **33**, 13874–13881 (2017).
5. T. Matsubara *et al.*, Amyloid-ß fibrils assembled on ganglioside-enriched membranes contain both parallel ß-sheets and turns. *J. Biol. Chem.* **293**, 14146–14154 (2018).
6. W. F. Zeno *et al.*, Synergy between intrinsically disordered domains and structured proteins amplifies membrane curvature sensing. *Nat. Commun.* **9**, 4152 (2018).
7. F. Yuan *et al.*, The ins and outs of membrane bending by intrinsically disordered proteins. *Sci. Adv.* **9**, eadg3485 (2023).
8. U. Kaur, J. C. Lee, Unroofing site-specific α-synuclein-lipid interactions at the plasma membrane. *Proc. Natl. Acad. Sci. U.S.A.* **117**, 18977–18983 (2020).
9. K. Simons, E. Ikonen, Functional rafts in cell membranes. *Nature* **387**, 569–572 (1997).
10. H. J. Risselada, S. J. Marrink, The molecular face of lipid rafts in model membranes. *Proc. Natl. Acad. Sci. U.S.A.* **105**, 17367–17372 (2008).
11. D. Lingwood, K. Simons, Lipid rafts as a membrane-organizing principle. *Science* **327**, 46–50 (2010).
12. K. Simons, J. L. Sampaio, Membrane organization and lipid rafts. *Cold Spring Harb. Perspect. Biol.* **3**, a004697 (2011).
13. E. Sezgin, I. Levental, S. Mayor, C. Eggeling, The mystery of membrane organization: Composition, regulation and roles of lipid rafts. *Nat. Rev. Mol. Cell Biol.* **18**, 361–374 (2017).
14. I. Levental, K. R. Levental, F. A. Heberle, Lipid rafts: Controversies resolved, mysteries remain. *Trends Cell Biol.* **30**, 341–353 (2020).
15. B. Maier, J. O. Rädler, Conformation and self-diffusion of single DNA molecules confined to two dimensions. *Phys. Rev. Lett.* **82**, 1911 (1999).
16. S. A. Sukhishvili *et al.*, Diffusion of a polymer 'pancake'. *Nature* **406**, 146–146 (2000).
17. S. A. Sukhishvili *et al.*, Surface diffusion of poly(ethylene glycol). *Macromolecules* **35**, 1776–1784 (2002).
18. T. G. Desai, P. Keblinski, S. K. Kumar, S. Granick, Molecular-dynamics simulations of the transport properties of a single polymer chain in two dimensions. *J. Chem. Phys.* **124**, 084904 (2006).
19. T. G. Desai, P. Keblinski, S. K. Kumar, S. Granick, Modeling diffusion of adsorbed polymer with explicit solvent. *Phys. Rev. Lett.* **98**, 218301 (2007).
20. T. G. Desai, P. Keblinski, S. K. Kumar, Polymer chain dynamics at interfaces: Role of boundary conditions at solid interface. *J. Chem. Phys.* **128**, 044903 (2008).
21. H. J. Qian, L. J. Chen, Z. Y. Lu, Z. S. Li, Surface diffusion dynamics of a single polymer chain in dilute solution. *Phys. Rev. Lett.* **99**, 068301 (2007).
22. D. Mukherji, G. Bartels, M. H. Müser, Scaling laws of single polymer dynamics near attractive surfaces. *Phys. Rev. Lett.* **100**, 068301 (2008).
23. J. S. Wong, L. Hong, S. C. Bae, S. Granick, Polymer surface diffusion in the dilute limit. *Macromolecules* **44**, 3073–3076 (2011).
24. J. Li, R. Zhang, M. Ding, T. Shi, Unusual self-diffusion behaviors of polymer adsorbed on rough surfaces. *J. Chem. Phys.* **150**, 064902 (2019).

25. L. Zhang, S. Granick, Slaved diffusion in phospholipid bilayers. *Proc. Natl. Acad. Sci. U.S.A.* **102**, 9118–9121 (2005).
26. D. Wang *et al*., Scaling of polymer dynamics at an oil-water interface in regimes dominated by viscous drag and desorption-mediated flights. *J. Am. Chem. Soc.* **137**, 12312–12320 (2015).
27. T. Taddese, D. L. Cheung, P. Carbone, Scaling behavior of polymers at liquid/liquid interfaces. *ACS Macro Lett.* **4**, 1089–1093 (2015).
28. P. Saffman, M. Delbrück, Brownian motion in biological membranes. *Proc. Natl. Acad. Sci. U.S.A.* **72**, 3111–3113 (1975).
29. B. H. Zimm, Dynamics of polymer molecules in dilute solution: Viscoelasticity, flow birefringence and dielectric loss. *J. Chem. Phys.* **24**, 269–278 (1956).
30. M. Rubinstein, R. Colby, *Polymer Physics* (Oxford University Press, 2003).
31. M. Fallahi-Sichani, J. J. Linderman, Lipid raft-mediated regulation of G-protein coupled receptor signaling by ligands which influence receptor dimerization: A computational study. *PLoS One* **4**, e6604 (2009).
32. M. Klacsová, A. Bóta, P. Balgavỳ, DOPC-DOPE composition dependent Lα-HII thermotropic phase transition: SAXD study. *Chem. Phys. Lipids* **198**, 46–50 (2016).
33. L. Tubiana, E. Orlandini, C. Micheletti, Multiscale entanglement in ring polymers under spherical confinement. *Phys. Rev. Lett.* **107**, 188302 (2011).
34. H. Arkın, W. Janke, Structural behavior of a polymer chain inside an attractive sphere. *Phys. Rev. E* **85**, 051802 (2012).
35. D. Marenduzzo, C. Micheletti, E. Orlandini, D. W. Sumners, Topological friction strongly affects viral DNA ejection. *Proc. Natl. Acad. Sci. U.S.A.* **110**, 20081–20086 (2013).
36. S. Dutta, P. Benetatos, Statistical ensemble inequivalence for flexible polymers under confinement in various geometries. *Soft Matter* **16**, 2114–2127 (2020).
37. A. J. Levine, T. Liverpool, F. C. MacKintosh, Dynamics of rigid and flexible extended bodies in viscous films and membranes. *Phys. Rev. Lett.* **93**, 038102 (2004).
38. S. Ramachandran, S. Komura, K. Seki, G. Gompper, Dynamics of a polymer chain confined in a membrane. *Eur. Phys. J. E* **34**, 1–13 (2011).
39. A. Boromand, S. Jamali, J. M. Maia, Viscosity measurement techniques in dissipative particle dynamics. *Comput. Phys. Commun.* **196**, 149–160 (2015).
40. P. Cicuta, S. L. Keller, S. L. Veatch, Diffusion of liquid domains in lipid bilayer membranes. *J. Phys. Chem. B* **111**, 3328–3331 (2007).
41. H. A. Faizi, R. Dimova, P. M. Vlahovska, A vesicle microrheometer for high-throughput viscosity measurements of lipid and polymer membranes. *Biophys. J.* **121**, 910–918 (2022).
42. J. E. Fitzgerald, R. M. Venable, R. W. Pastor, E. R. Lyman, Surface viscosities of lipid bilayers determined from equilibrium molecular dynamics simulations. *Biophys. J.* **122**, 1094–1104 (2023).
43. J. Ma *et al*., Tuning extracellular fluid viscosity to enhance transfection efficiency. *Nat. Chem. Eng.* **1**, 576–587 (2024).
44. S. Ramadurai *et al*., Lateral diffusion of membrane proteins. *J. Am. Chem. Soc.* **131**, 12650–12656 (2009).
45. K. Weiß *et al*., Quantifying the diffusion of membrane proteins and peptides in black lipid membranes with 2-focus fluorescence correlation spectroscopy. *Biophys. J.* **105**, 455–462 (2013).
46. B. Hughes, B. Pailthorpe, L. White, The translational and rotational drag on a cylinder moving in a membrane. *J. Fluid Mech. Res.* **110**, 349–372 (1981).
47. J. F. Klingler, H. M. McConnell, Brownian motion and fluid mechanics of lipid monolayer domains. *J. Phys. Chem.* **97**, 6096–6100 (1993).
48. S. A. Shelby, I. Castello-Serrano, K. C. Wisser, I. Levental, S. L. Veatch, Membrane phase separation drives responsive assembly of receptor signaling domains. *Nat. Chem. Biol.* **19**, 750–758 (2023).
49. M. Rouches, S. L. Veatch, B. B. Machta, Surface densities prewet a near-critical membrane. *Proc. Natl. Acad. Sci. U.S.A.* **118**, e2103401118 (2021).
50. L. Li *et al*., Influence of lipid rafts on pattern formation during T-cell adhesion. *New J. Phys.* **23**, 043052 (2021).
51. N. Fricke *et al*., High-content imaging platform to discover chemical modulators of plasma membrane rafts. *ACS Cent. Sci.* **8**, 370–378 (2022).
52. K. Seki, S. Komura, M. Imai, Concentration fluctuations in binary fluid membranes. *J. Phys. Condens. Matter* **19**, 072101 (2007).
53. A. Naji, A. J. Levine, P. A. Pincus, Corrections to the Saffman-Delbrück mobility for membrane bound proteins. *Biophys. J.* **93**, L49–L51 (2007).
54. Y. Gambin *et al*., Lateral mobility of proteins in liquid membranes revisited. *Proc. Natl. Acad. Sci. U.S.A.* **103**, 2098–2102 (2006).
55. H. Turlier, T. Betz, Unveiling the active nature of living-membrane fluctuations and mechanics. *Annu. Rev. Condens. Matter Phys.* **10**, 213–232 (2019).
56. P. Hoogerbrugge, J. Koelman, Simulating microscopic hydrodynamic phenomena with dissipative particle dynamics. *Europhys. Lett.* **19**, 155 (1992).
57. P. Espanol, P. Warren, Statistical mechanics of dissipative particle dynamics. *Europhys. Lett.* **30**, 191 (1995).
58. R. D. Groot, P. B. Warren, Dissipative particle dynamics: Bridging the gap between atomistic and mesoscopic simulation. *J. Chem. Phys.* **107**, 4423–4435 (1997).
59. P. Español, Hydrodynamics from dissipative particle dynamics. *Phys. Rev. E* **52**, 1734–1742 (1995).
60. Y. Kong, C. Manke, W. Madden, A. Schlijper, Effect of solvent quality on the conformation and relaxation of polymers via dissipative particle dynamics. *J. Chem. Phys.* **107**, 592–602 (1997).
61. W. Jiang, J. Huang, Y. Wang, M. Laradji, Hydrodynamic interaction in polymer solutions simulated with dissipative particle dynamics. *J. Chem. Phys.* **126**, 044901 (2007).
62. M. Laradji, P. Sunil Kumar, Dynamics of domain growth in self-assembled fluid vesicles. *Phys. Rev. Lett.* **93**, 198105 (2004).
63. J. C. Shillcock, R. Lipowsky, Tension-induced fusion of bilayer membranes and vesicles. *Nat. Mater.* **4**, 225–228 (2005).
64. A. Grafmüller, J. Shillcock, R. Lipowsky, Pathway of membrane fusion with two tension-dependent energy barriers. *Phys. Rev. Lett.* **98**, 218101 (2007).
65. J. Hu, R. Lipowsky, T. R. Weikl, Binding constants of membrane-anchored receptors and ligands depend strongly on the nanoscale roughness of membranes. *Proc. Natl. Acad. Sci. U.S.A.* **110**, 15283–15288 (2013).
66. J. A. Anderson, J. Glaser, S. C. Glotzer, Hoomd-blue: A python package for high-performance molecular dynamics and hard particle Monte Carlo simulations. *Comput. Mater. Sci.* **173**, 109363 (2020).
67. C. L. Phillips, J. A. Anderson, S. C. Glotzer, Pseudo-random number generation for Brownian dynamics and dissipative particle dynamics simulations on GPU devices. *J. Comput. Phys.* **230**, 7191–7201 (2011).
68. Y. L. Zhu *et al*., GALAMOST: GPU-accelerated large-scale molecular simulation toolkit. *J. Comput. Chem.* **34**, 2197–2211 (2013).
69. Y. L. Zhu *et al*., Employing multi-GPU power for molecular dynamics simulation: An extension of GALAMOST. *Mol. Phys.* **116**, 1065–1077 (2018).
70. M. Yang *et al*., Gel phase membrane retards amyloid ß-peptide (1–42) fibrillation by restricting slaved diffusion of peptides on lipid bilayers. *Langmuir* **34**, 8408–8414 (2018).
71. J. Gao, J. Hu, Python scripts. GitHub. (2025) https://github.com/JieGao-web/polymer_sailing_on_rafts. Deposited May 19, 2025.